Electron sources in Saturn's magnetosphere

A. M. Rymer,[1] B. H. Mauk,[1] T. W. Hill,[2] C. Paranicas,[1] N. André,[3] E. C. Sittler Jr.,[4] D. G. Mitchell,[1] H. T. Smith,[5] R. E. Johnson,[5] A. J. Coates,[6] D. T. Young,[7] S. J. Bolton,[7] M. F. Thomsen,[8] and M. K. Dougherty[9]

Received 10 August 2006; revised 19 October 2006; accepted 30 October 2006; published 9 February 2007.

[1] We investigate the sources of two different electron components in Saturn's inner magnetosphere ($5 < L < 12$ Rs) by performing phase space density ($f(v)$) analyses of electron measurements made by the Cassini CAPS instrument (1 eV to 28 keV). Because pitch angle distributions indicate that the traditional single particle invariants of gyration and bounce are not appropriate, we use a formulation of the isotropic invariant derived by Wolf (1983) and Schulz (1998) and show that it is similar in functional form to the first adiabatic invariant. Our $f(v)$ analyses confirm that the cooler electrons (<100 eV) have a source in the inner magnetosphere and are likely products of neutral ionization processes in Saturn's neutral cloud. The mystery is how the electrons are heated to energies comparable to the proton thermal energy (which is approximately equal to the proton pickup energy), a process that reveals itself as a source of electrons at given invariant values in our $f(v)$ analyses. We show that Coulomb collisions provide a viable mechanism to achieve the near equipartition of ion and electron energies in the time available before particles are lost from the region. We find that the source of the hotter electron component (>100 eV) is Saturn's middle or outer magnetosphere, perhaps transported to the inner magnetosphere by radial diffusion regulated by interchange-like injections. Hot electrons undergo heavy losses inside $L \sim 6$ and the distance to which the hot electron component penetrates into the neutral cloud is energy-dependent, with the coolest fraction of the hot plasma penetrating to the lowest L-shells. This can arise through energy-dependent radial transport during the interchange process and/or loss through the planetary loss cone.

Citation: Rymer, A. M., et al. (2007), Electron sources in Saturn's magnetosphere, *J. Geophys. Res.*, *112*, A02201, doi:10.1029/2006JA012017.

1. Introduction

[2] The Cassini plasma spectrometer (CAPS) aboard the Cassini spacecraft provides electron and ion energy spectra from less than 1 eV to tens of keV (along with directional information). As reported by *Young et al.* [2005] in a study of plasma sources and transport observed by CAPS during Cassini's first orbit of Saturn (June/July 2004), bimodal electron energy distributions are often observed between approximately 5 and 12 Rs (Rs = Saturn's radius ~60,300 km) from Saturn. The two populations consist of a cold component (1–100 eV) and a hot component (1–100 keV). These were first observed in Voyager 1 and 2 plasma data as reported by *Sittler et al.* [1983] and later by *Maurice et al.* [1996]. CAPS measures lower energies than the Voyager plasma science experiment and both *Young et al.* [2005] and *Sittler et al.* [2005, 2006] confirm *Sittler et al.*'s [1983] original inference that the cold electron component exists below 10 eV within the orbit of Dione at about 6.3 Rs.

[3] Notable other instances of bimodal electron energy distributions in the solar system are the core/halo solar wind components [e.g., *Feldman et al.*, 1975], the Io plasma torus [*Scudder et al.*, 1981; *Sittler and Strobel*, 1987; *Frank and Paterson*, 2000] and thin boundary layers such as at planetary magnetopauses [e.g., *Lundin*, 1988]. In the Io torus it is likely that the colder electron population is an ionization product of pickup gases from Io. Given its field-aligned character, the hotter component may be produced by the field-aligned currents that regulate radial transport via interchange.

[1]Johns Hopkins University Applied Physics Laboratory, Laurel, Maryland, USA.
[2]Department of Physics and Astronomy, Rice University, Houston, Texas, USA.
[3]Research and Scientific Support Department, European Space Agency, Noordwijk, Netherlands.
[4]NASA Goddard Space Flight Center, Greenbelt, Maryland, USA.
[5]University of Virginia, Charlottesville, Virginia, USA.
[6]Mullard Space Science Laboratory, University College London, London, UK.
[7]Southwest Research Institute, San Antonio, Texas, USA.
[8]Space and Atmospheric Science Group, Los Alamos National Laboratory, Los Alamos, New Mexico, USA.
[9]Department of Space and Atmospheric Physics, Imperial College London, London, UK.

Copyright 2007 by the American Geophysical Union.
0148-0227/07/2006JA012017

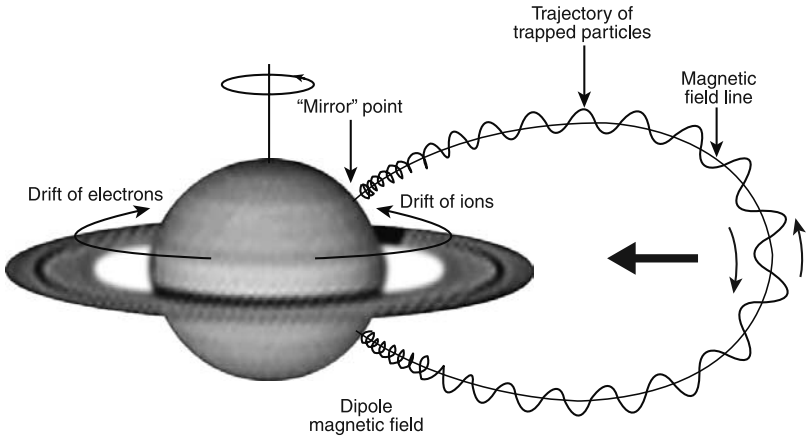

Figure 1. Cartoon illustrating ideal plasma transport at Saturn showing the trajectory a particle might follow as it travels along and around a magnetic field line along with the drift of electrons and ions in Saturn's magnetic field [after *Mitchell*, 2000].

[4] Electron injection events are a prevalent feature of Saturn's inner magnetosphere and are often attributed to the centrifugal interchange instability [*André et al.*, 2005; *Burch et al.*, 2005; *Hill et al.*, 2005; *Leisner et al.*, 2005; *Mauk et al.*, 2005]. Such interchanges are thought to be regulated by interaction with the planetary ionosphere through the intermediary of field-aligned currents [e.g. *Richardson and Siscoe*, 1981; *Huang and Hill*, 1991]. Thus there are two independent sources of suprathermal electrons associated with the interchange process; they may be produced locally by field-aligned currents that accompany interchange, or they may be accelerated in the outer magnetosphere and transported inward. Figure 1 shows a schematic illustrating this latter hypothesis.

[5] Since the cold electron component at Saturn exists in approximately the same region as Saturn's neutral cloud [*Richardson et al.*, 1998; *Johnson et al.*, 2006], it seems likely that these electrons have a local source associated with plasma-neutral interactions. We test these hypotheses using phase space density analysis of data from the Cassini Electron Spectrometer [*Linder et al.*, 1998; *Young et al.*, 2004].

2. Procedure

[6] To understand sources of charged particles, we follow the traditional approach of converting our data to phase space densities and binning these by invariants. One simple invariant is the particle flux tube content: in the absence of sources and sinks, radial transport by $\mathbf{E} \times \mathbf{B}$ drift should conserve

$$\eta \equiv \int n ds/B \tag{1}$$

for a given species, where n is the number density of that species, B is magnetic field strength, and s is distance along B. The integral is along the magnetic field line. Several studies have reported results of this type of analysis for Saturnian plasma distributions by examining the simplification of (1) for a dipolar field, NL^2, versus L, where N is the total number of ions per shell of magnetic flux and L is the equatorial crossing distance of the field line normalized to Rs, and looking for sources and sinks of particles as identified by maxima and minima within the NL^2 profile [*Richardson*, 1986; *Richardson and Sittler*, 1990; *Barbosa*, 1990; *Richardson*, 1992]. However, for the problem at hand we have multiple plasma components with no robust approach to assure that the densities of the respective populations are properly assigned. Instead, we choose to make use of the expected invariance of the electron phase space density, $f(v)$, of the particle populations when represented as functions of the single-particle adiabatic invariants so that the different energy components can be tracked separately in the same way.

[7] In the absence of pitch angle scattering, the first (gyration) adiabatic invariant

$$\mu = p_\perp^2/2mB (\rightarrow E_\perp/B \text{ non-relativistically}) \tag{2}$$

is expected to be conserved during radial transport (where $p_\perp$ and $E_\perp$ are momentum and energy perpendicular to $\mathbf{B}$). Likewise, in the absence of bounce-resonant field variations, the second (bounce) adiabatic invariant

$$J = \int p_\parallel ds \tag{3}$$

is expected to be conserved (where $p_\parallel$ is momentum parallel to $\mathbf{B}$ and the integral is over a complete bounce cycle). In the present work we will use the first adiabatic invariant as a point of reference. However, we have found by inspection that, while anisotropic electron pitch angle distributions are observed (J. L. Burch et al., Tethys and Dione: Sources of outward flowing plasma in Saturn's magnetosphere, submitted to *Nature*, 2007, hereinafter referred to as Burch et al., submitted manuscript, 2007), the distributions are generally too nearly isotropic to be consistent with conservation of the first and second adiabatic invariants. To illustrate this, the solid curve in Figure 2 has been constructed by moving an isotropic pitch angle distribution

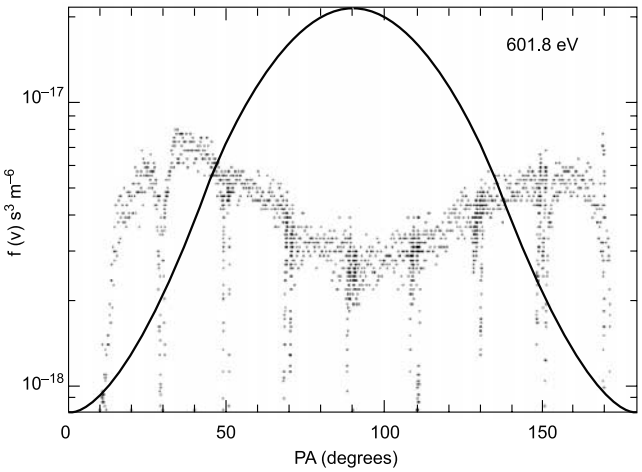

Figure 2. Solid curve shows the expected pitch angle evolution as electrons are moved from L = 15 to L = 5 conserving the first and second adiabatic invariants. Overplotted dots show the angular distribution of 610.8 eV electrons measured by Cassini-ELS at 1910–1920 on 28 October 2004.

from L = 15 to L = 5 assuming an isotropic source at L = 15 with $f(v) \propto E^{-3}$, consistent with CAPS observations at that distance. We see that the expected pitch angle variation associated with this motion results in spectra differing by a factor of greater than 25 from peak to trough. Example $f(v)$ versus pitch angle spectra for 602 eV electrons measured by the Cassini-ELS 1910–1920 UT on 28 October 2004 are overplotted in Figure 2. The observed electron angular distributions resemble a "butterfly" distribution rather than the expected "pancake" distribution and vary, typically, by less than a factor of three. The data shown here overlap with those shown by Burch et al. (submitted manuscript, 2007), who propose an explanation for the observed distributions in terms of plasma outwelling.

[8] Our approach is to assume that the electrons undergo sufficiently strong, but elastic, pitch angle scattering such that they isotropize without significantly changing in energy. With these assumptions we can, for each energy E, treat each unit of plasma as an ideal gas volume. Using the familiar ideal gas laws:

$$PV = NkT \tag{4}$$

and

$$PV^{\gamma} = \text{constant}, \tag{5}$$

where $\gamma = (k + 2)/k$ and k is the number of degrees of freedom (k = 3 for an ideal gas). Substituting the pressure P from (4) into (5), we have $(NkT/V)V^{\gamma}$ = constant, then equating kT to particle energy, $E(=p^2/2m$ relativistically), and combining total density, N, into a new constant, C, we write:

$$EV^{\gamma-1} = \frac{p^2}{2m}V^{2/3} = C \tag{6}$$

where p and E are total momentum and energy, and

$$V = \int ds/B \tag{7}$$

is the flux tube volume per unit magnetic flux [e.g., *Wolf*, 1983; *Schulz*, 1998]. In a dipole field, $V \propto L/B_{eq} \propto L^4$, where B_{eq} is the field strength at the equatorial crossing distance, resulting in $E \propto L^{-8/3}$ (cf. $E_{\perp} \propto L^{-3}$ for μ conservation and $E_{\parallel} \propto L^{-2}$ for J conservation). Here we will use the left-hand side of (6), correct only in the nonrelativistic limit, with $V \propto L/B_{eq}$ but we will use the measured value of B from the Cassini flux gate magnetometer [*Dougherty et al.*, 2004]. Thus we incorporate most of the correction due to the radial stretching of the field, with the remaining error just roughly linearly proportional to the assigned value of L. (To incorporate the other part of this correction, we would need to integrate along a global model of the distorted field, which is not presently available). Substituting these parameters into the left-hand side of (6), we find

$$\Lambda = E(L/B)^{2/3} = C \tag{8}$$

which we refer to as the "isotropic invariant" and is equivalent (after taking the 2/3 power of both sides) to that defined by *Schulz* [1998]. With E replaced by kT, this is the same result used by other authors to track the evolution of the mean energy of entire populations in Uranus' magnetosphere [*Belcher et al.*, 1991]. Our approach differs in that we use (8) separately for each energy of the distribution, under the assumption that scattering predominantly changes the pitch angles of the particles and not their energies and so, as discussed by *Schulz* [1998], conservation of this invariant does not couple particles with different energies on the same flux tube. For the CAPS energies considered here (1 eV to 28 keV), the nonrelativistic version of (6) is adequate. In future work, we will extend this study to the higher-energy particles measured by the Cassini MIMI instrument [*Krimigis et al.*, 2004], which will require the relativistic version of (6). Note that when expressed as functions of L for a purely dipolar configuration, the first adiabatic invariant (EL^3 = constant) is quite close to our isotropic invariant ($EL^{8/3}$ = constant). Our subsequent analysis therefore is broadly appropriate in terms of conservation of both μ and Λ. This result is achieved despite the fact that strong scattering strongly violates the conditions that give rise to the assumed stability of the first and second invariants.

[9] Phase space density, $f(v)$, is related to the observed differential intensity I (cm^{-2} s^{-1} sr^{-1} eV^{-1}) by the relation $f(v)$ = const $\times$ I/p^2. A particle whose motion conserves invariants (μ, J, or Λ) in a known field will trace a predictable trajectory in particle energy space. We test this expectation by extracting $f(v)$ along lines of constant isotropic invariant, Λ. Inherent in this procedure is the assumption that the phase space density derived from particle intensities in Saturn's equatorial plane at constant invariant is a conserved quantity under radial transport in the absence of sources and losses. This is a common assumption in the case of a collisionless plasma, where

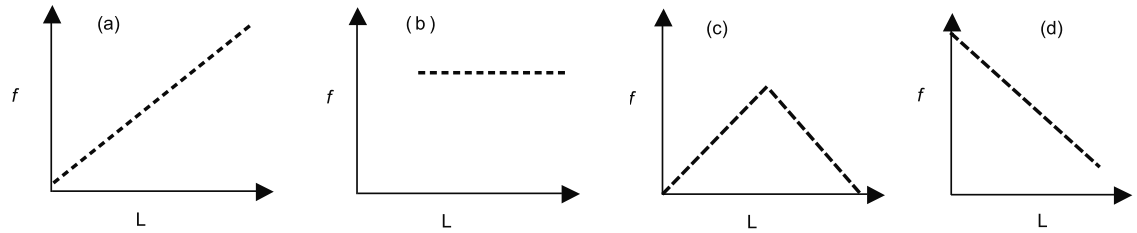

Figure 3. Cartoons illustrating different phase space density profiles, f, versus L for (a) an external source, (b) very rapid radial transport, (c) an embedded source with external and internal sinks, and (d) an internal source and external sink.

we neglect the collisional terms of the Boltzmann equation to derive Liouville's theorem. Even given the assumed strong pitch angle scattering condition, our assumption of a collisionless plasma is formally valid if the scattering agent is wave-particle interactions with waves supported by the collective behavior of large numbers of particles. We assume it to be approximately valid irrespective of the scattering agent.

[10] *Green and Kivelson* [2004] provide a comprehensive recent description of how different $f(v)$ versus L profiles can arise. Some sample profiles are shown schematically in Figure 3. Figure 3a shows the classical expectation that results from an external source of particles, an internal region of loss, and diffusive radial transport. The loss region may be distributed but is only actually required at the innermost position. Diffusive transport yields variations of $f(v)$, even while preserving adiabatic invariants because the $f(v)$ value at any one position represents the mixing of flux tubes from larger L that are relatively full of particles and those from smaller L that are relatively empty of particles. The presence of distributed losses makes the slope steeper than it would otherwise be. In the absence of sources and losses, diffusive radial transport is described by

$$\frac{D_{LL}}{L^2}\frac{df}{dL} = \text{constant} \tag{9}$$

[*Van Allen et al.*, 1980], where D_{LL} is the classical radial diffusion coefficient. So if D_{LL} is very large, df/dL must be small, and $f(v)$ will be flat (Figure 3b). A flat $f(v)$ profile (Figure 3b) can also occur if the transport in a given region is coherent (e.g., convection) rather than diffusive or if there exists a distributed source across the region. A peaked profile, as illustrated in Figure 3c, indicates that there exists a source at the peak, diffusive transport away from that source, and both planetward and external sinks. Again, for diffusive transport in the absence of distributed losses, the slopes away from the source position depend on the magnitude of the transport coefficient relative to the source strength. A final example for an internal source and an external sink is shown in Figure 3d.

[11] Several previous studies have analyzed in situ Saturn plasma data from the Pioneer and Voyager flybys in terms of the first and second adiabatic invariants [*McDonald et al.*, 1980; *Van Allen et al.*, 1980; *Armstrong et al.*, 1983; *Maurice et al.*, 1996]. Most of these previous studies addressed particle energies much higher than those considered here, although Maurice et al. included lower-energy particles that overlapped the energy range considered here. The results of these previous studies were generally consistent with inward diffusion of energetic particles from an external source, together with an internal plasma source at $L < 4$.

3. Observations

[12] We considered data from five Cassini orbits listed in Table 1 (see *Mitchell* [2000] for a description of the mission and orbital designations). All data were taken within $L = 15$ and the maximum/minimum latitudes sampled in this range are shown in the last column. Within the radial range considered, Cassini was within 5 Rs of Saturn's equatorial plane.

[13] Figure 4 shows CAPS electron data from the well-documented Saturn orbit insertion (SOI) orbit on the left-hand side and the almost equatorial Rev4 orbit on the right-hand side. All data presented and analyzed here have been corrected by a positive "correction potential" (analogous to spacecraft potential) where possible. Inside of $L \sim 6$ the spacecraft potential typically becomes negative as more magnetospheric electrons flow onto the spacecraft than photoelectrons flow off it; in this case the appropriate correction potential is unknown and the $f(v)$ is likely underestimated [*Rymer*, 2004]. The top panels of Figure 4 show energy versus dipolar L with the measured count rates indicated by the color bars; the $f(v)$ derived from these count rates is shown in the same format on the bottom panels. The overplotted white lines represent lines of constant μ and Λ (solid and dashed lines, respectively). The overplotted blue dashed lines indicate the proton corotation energy.

[14] Because raw counts represent roughly energy flux, not number flux, the energy dependence in Figure 4b is modified from that in Figure 4a by a factor of $1/E^2$. The $1/E^2$ dependence of $f(v)$ somewhat masks the bimodal electron populations. To illustrate quantitively the bimodal

Table 1. Cassini Orbits Included in the Present Analysis

Orbit Name	Start Date (DOY)	End Date (DOY)	Max./Min. Latitude, deg
SOI	30 Jun (182) 2004	1 Jul (183) 2004	17.1, −14.4
RevA	27 Oct (301) 2004	29 Oct (303) 2004	13.8, −9.6
RevB	13 Dec (348) 2004	16 Dec (351) 2004	5.2, −4.8
Rev4	15 Feb (046) 2005	18 Feb (049) 2005	0.41, −0.42
Rev5	8 Mar (067) 2005	10 Mar (069) 2005	0.21, −0.21

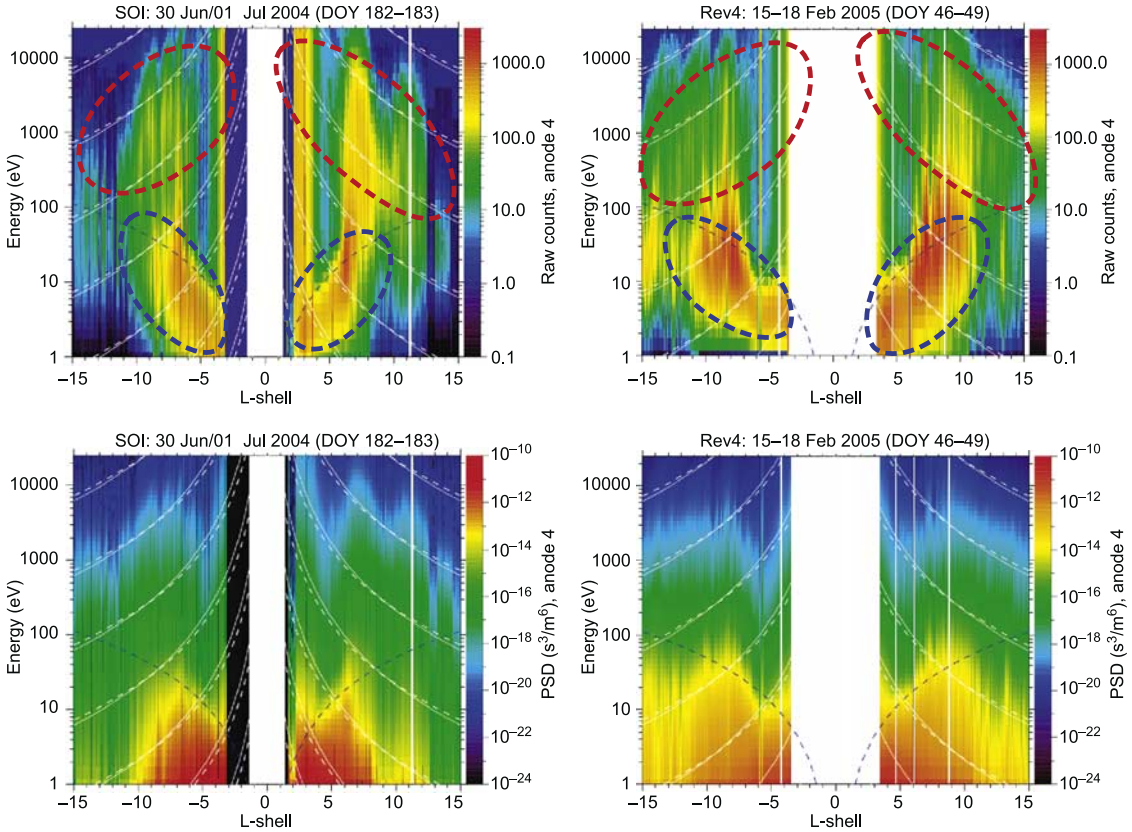

Figure 4. CAPS-ELS data from SOI and Rev4. (top) Electron count rate corrected for spacecraft potential. We have overplotted red and blue ovals to emphasize hot and cold components referred to in the text. (bottom) Derived phase space density. Overplotted white solid/dashed lines on both panels are lines of constant μ and Λ, respectively. Overplotted blue dashed lines indicate the corotation energy appropriate to a picked-up proton.

nature first revealed by *Young et al.* [2005], Figure 5 shows several counts-versus-energy spectra measured in the inner magnetosphere during SOI and Rev 4.

[15] We used data like those shown in Figure 4b to generate the profiles shown in Figure 6. Each panel shows the *f(v,L)* extracted along a different value of Λ, with inbound and outbound data overplotted in red and blue, respectively. As with Figure 4, data on the left are from the SOI orbit and on the right from the nearly equatorial Rev4 orbit. For ease of reference, Table 2 provides the electron energy appropriate to the values of Λ presented for a few values of L-shell.

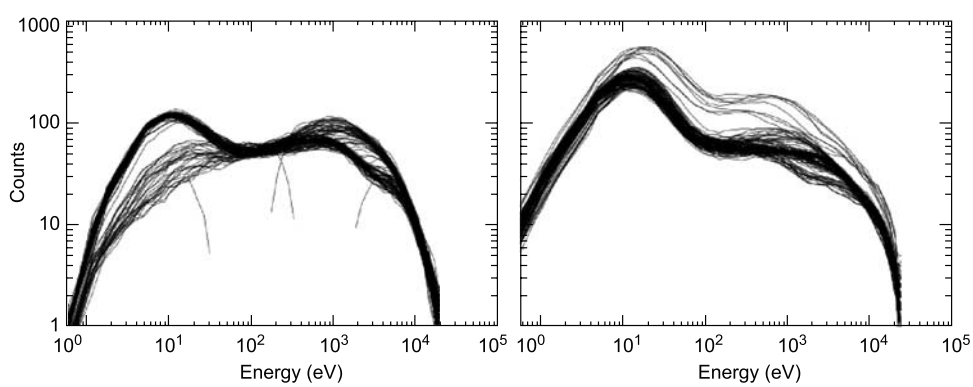

Figure 5. Counts versus energy spectra showing bimodal electron distributions in Saturn's inner magnetosphere. Each plot shows 100 consecutive traces, SOI (LHS) from around $L = 8$, and Rev4 (RHS) around $L = 11$.

Table 2. Electron Energies Appropriate to Our Value of the Isotropic Invariant, Λ, at Different L Values

Λ, eV(Rs/T)$^{2/3}$	Electron Energy at L = 12, eV	Electron Energy at L = 10, eV	Electron Energy at L = 8, eV	Electron Energy at L = 6, eV
1e9	1.1	2	3.8	8
1e10	11	20	38	80
1e11	110	200	380	800
1e12	1100	2000	3800	8000

[16] Our initial inspection of the SOI data at low energies was suggestive of a peaked profile, consistent with a plasma source in the range $6 < L < 9$. However, inspection of subsequent, more equatorial orbits (e.g., Rev4, Figure 5, right), indicates that the apparent peak was probably in fact part of a plateau region and that the fall off observed beyond $L \sim 9$ during SOI was likely the result of Cassini's excursion to relatively high latitudes with respect to a more equatorially confined transport region (plasma sheet). We therefore focus our discussion on data taken during Rev4 on the assumption that this provides better insight into equatorial plasma processes because the spacecraft remains close to the equator throughout the region of interest. Rev5 was similarly confined very near the equator, following an almost identical trajectory to Rev4, and the following discussion applies equally well to both orbits.

4. Discussion

4.1. "Cold" Electron Population (<∼100 eV)

[17] It is evident from the top panels of Figure 4 that the "cold" electron population (indicated approximately by the blue ovals) does not track any line of constant invariant, quite the opposite in fact. *Young et al.* [2005] and *Sittler et al.* [2006] show that the low-energy electrons approximately track the proton temperature (and corotation energy). We find, from examination of all orbits considered in the present analysis, that the cold plasma radial profile is not consistent with lossless transport that conserves the isotropic invariant. This condition suggests that there exists a local source inside $L \sim 11$ for these electrons for which radial transport is small compared with the production rate and that this source exists to low L values, at least to $L \sim 4$. We also observe that the energy of the cold electron component approaches, approximately, the proton corotation energy, as indicated by the blue dashed line on the panels of Figure 4.

[18] Saturn's neutral cloud [*Jurac et al.*, 2002; *Jurac and Richardson*, 2005; *Johnson et al.*, 2005] is a likely source for the cold plasma component which could be formed as a product of impact ionization and/or photoionization. If we assume that the ionization results in the creation of a cold ion and electron then both will be quickly picked up to the local corotation speed, with an ion/electron energy partition equal to the ratio of ion to electron mass (i.e., the electrons will start out being very cold). *Sittler et al.* [2006] suggest that Coulomb collisions will heat the thermal electrons, we explore that in more detail here. The electrons and positive ions all move together at (or approaching) the corotation velocity, so the equilibration occurs in the (partially) corotating frame and transfers energy from ion temperature to electron temperature. Given a mixture of ions and electrons with different temperatures the amount of time (1 e-folding time) needed for electrons at temperature, T_e, to equilibrate with ions at temperature, T_i, based solely on Coulomb collisions, was described by *Spitzer* [1962] and is given by

$$\tau_{eq}^{e/i} = \frac{(\mu_e T_i + \mu_i T_e)^{3/2}}{(\mu_e \mu_i)^{1/2} Z_i^2 n_i \lambda_{e/i}} \sec \tag{10}$$

where μ_e and μ_i are the electron and ion mass, respectively, in units of the proton mass, m_p, Z_i is the ion charge state, and $\lambda_{e/i}$ is the Coulomb logarithm, temperatures are in electron volts and densities cm^{-3}. The Coulomb logarithm for electron ion collisions where $\mu_e \rightarrow 0$ and $T_p \mu_e < T_e < \sim 10$ eV (taken from *Book* [1981]) is

$$\lambda_{e/i} = 23 - \ln\left(n_e^{1/2} Z_i T_e^{-3/2}\right) \tag{11}$$

Figure 7 shows the results for $\tau_{eq}^{e/i}$in hours versus L-shell with T_i equal to the proton corotation energy and an assumed electron start energy, T_e, of 0.5 eV. We find that it will take tens of Saturn rotations for 0.5 eV electrons to equilibrate with protons at the proton corotation energy through Coulomb collisions alone; 153 hours at $L \sim 8$. We can ascertain roughly if this long timescale eliminates Coulomb collisions as the operable mechanism by considering the ion production rate compared to the resident ion density. Consider a toroidal region from $L = 4$ to $L = 10$ and with a height of 2 R_s; assuming a rectangular cross section, this torus has a volume of 2×10^{32} cm^3. We estimate the average charged particle density across the volume to be $n_e = n_i = 10$ cm^{-3} (from a combination of CAPS and RPWS measurements [*Young et al.*, 2005; *Gurnett et al.*, 2005]), corresponding to a total charged particle content, n_{tot}, of 2×10^{33}. From estimates of a neutral source rate of $\sim 10^{28}$ s^{-1}, of which 60–70% are lost to the outer magnetosphere [*Jurac and Richardson*, 2005; *Johnson et al.*, 2005], we assume an ion production rate, dn_{tot}/dt, of a few times 10^{27} s^{-1}. The lifetime against ion transport from the region, to maintain a steady state, is then $(n_{tot}/dn_{tot})dt \sim 10^6$ s. This means that to maintain the observed plasma density typical plasma ion or electron lifetimes are on the order of 300 hours. Given the rough estimates used this comparison of timescales suggests that the equipartitioning of energy via Coulomb collisions should not be ruled out.

[20] With the above analysis in mind, we now go on to discuss the $f(v)$ extracted at the lowest value of Λ (Figure 6a). Considering the data in this format we observe a plateau between $L \sim 6$ and $L \sim 11$. As we described earlier, a flat profile can arise (1) if D_{LL} is large compared to the source rate, i.e., there is very rapid diffusion, (2) if the plasma transport is superposed on a distributed plasma source, or (3) if there exists large-scale coherent transport. The coherent transport hypothesis seems the least likely

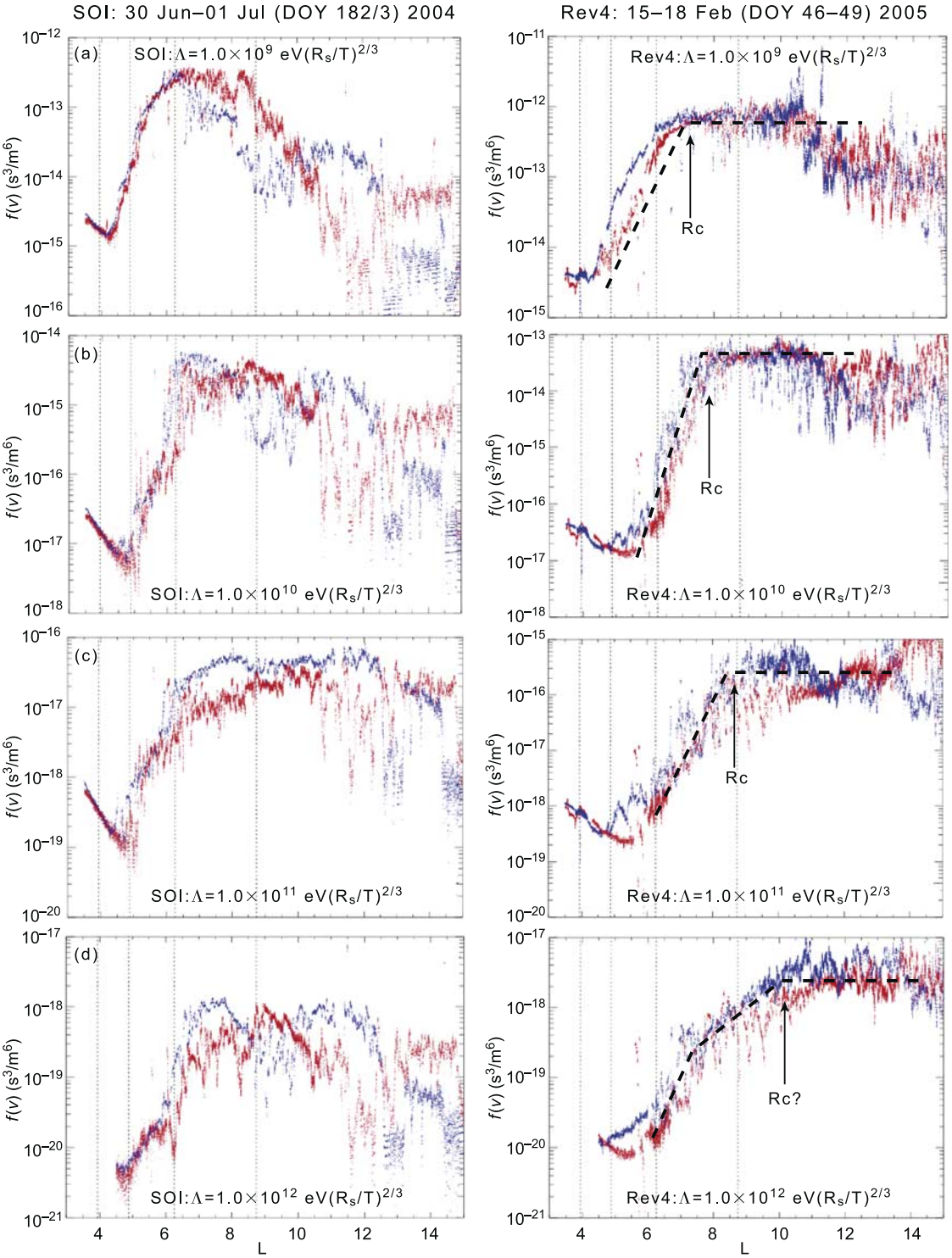

Figure 6. Phase space density versus L for selected values of isotropic energy invariant during the SOI orbit (left) and the Rev4 orbit (right). Red is inbound and blue is outbound. The strong positive gradient inside $L \sim 5$ is due to the onset of penetrating radiation in Saturn's radiation belts and so we cannot conclude anything about the transport in this region at present. The overplotted dashed lines are, from the left, respectively the orbital distances of the moons Enceladus, Tethys, Dione, and Rhea. The value of Λ appropriate to each plot is also shown.

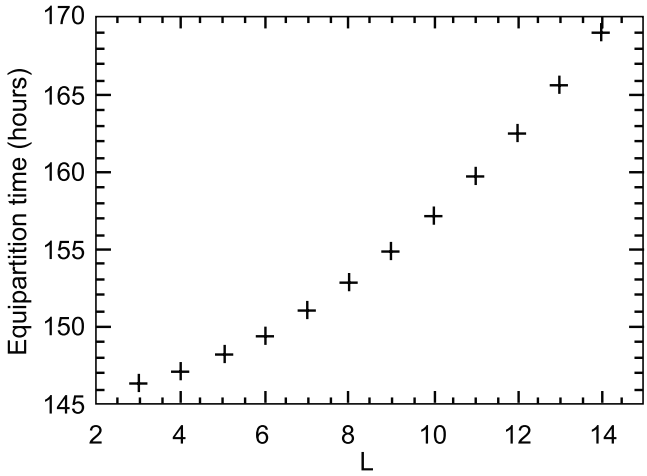

Figure 7. Equipartition time, described in the text, versus L-shell.

because of the rough symmetry observed between the inbound and outbound data (if a wind blows planetward at one azimuthal position, it must blow antiplanetward at other azimuthal positions). Note the dip in the phase space density profile outside $L \sim 11$. Electrons energized in the outer magnetosphere can not move across this gap under conditions of conservative transport. These observations are therefore not consistent with rapid inward transport from an external source for the lower-energy electrons.

[21] Our observations therefore suggest that there is either a distributed source inside $L \sim 11$, or a more localized source near $L \sim 7$ along with rapid outward transport and slow inward transport. The latter hypothesis is analogous to what happens at the Io torus, where rapid outward transport is driven by the centrifugal interchange instability and slower inward transport is presumably driven by planetary atmospheric turbulence [*Richardson and Siscoe*, 1981]. Our analysis, however, suggests that the former hypothesis is more likely at Saturn, with a distributed source(s) of electrons (and ions) inside $L \sim 11$, at least for these lower-energy particles. Our analysis also suggests that the source of these eV to tens of eV electrons is the heating of <1 eV electrons (thereby violating their local invariants) to energies of the order of the proton corotation energy.

[22] Inward of around the orbit of Dione the $f(v)$ profile switches from a flat to a negative gradient, labeled *Rc* on Figure 6a. This happens close to where the proton corotation energy (blue dashed line on Figure 4) crosses this line of invariant (second lowest white dashed line on Figure 4). Inspection of the top panels of Figure 4 suggests the electron source continues inward to at least $L \sim 4$, supplying electrons with energy appropriate to this value of Λ across only a limited range of L-shells. Note this is contrary to the usual interpretation, where a negative gradient arises due to an external source and an internal loss (Figure 3a). So, while our subsequent discussion will show that there are indeed losses which become significant at this distance, in the case of the lowest-energy electrons the source (most likely) continues to lower L but supplies electrons with energy below that appropriate to this value of Λ from $L \sim 6$. This illustrates that it is important to consider data in both formats to avoid overinterpretation or misinterpretation of the results.

4.2. Hot (>∼100 eV) Electron Component

[23] Higher-energy electrons show a tendency to increase in energy with decreasing L in a way that could be consistent with lossless, invariant-conserving transport (shown roughly within the red dashed ovals on Figure 4). As we consider higher values of Λ, we see a flatter phase space density profile from distance *Rc* to beyond $L = 15$ (Figures 6b–6d). There is no obvious local source for these electrons and so the plateau in $f(v)$ at higher energies is most likely due to the existence of a large D_{LL}, i.e., there exists rapid transport rather than convection or a distributed source of hot electrons. This transport may be due to the centrifugal interchange instability, CII. Heavy inner magnetospheric plasma goes outward and hotter tenuous flux tubes transport inward. Locally, this is manifest as a sudden depletion of cold plasma and appearance of hot plasma as reported by *Burch et al.* [2005]. The hot plasma subsequently gradient and curvature drifts out of the injected flux tube across flux tubes containing the locally produced cold electrons, as described by *Hill et al.* [2005]. We now know that Enceladus is a major source of neutrals (and therefore charged particles) [*Hansen et al.*, 2006; *Pontius and Hill*, 2006; *Porco et al.*, 2006; *Spahn et al.*, 2006; *Tokar et al.*, 2006; *Waite et al.*, 2006] and so we expect the CII to be observed all the way in to the Enceladus L-shell at L approximately 4. In this case our observation that the hot counterpart of the CII falls off heavily inward from about Dione's orbit at $L \sim 6$ is presumably due to enhanced losses that arise naturally at lower values of L (see later discussion), perhaps accentuated with wave-particle scattering stimulated by the cold plasmas that arise from Saturn's neutral gas clouds in this region.

[24] We observe that the transport in to the positions labeled *Rc* in Figure 7 and/or plasma losses inward of *Rc* are energy-dependent with the inner edge of the plateau apparently increasing in L with increasing Λ, that is the cooler part of the hot electron component is transported to lower L-shells than is the hotter plasma. We suggest that this condition arises from two mechanisms: (1) as a natural consequence of the invoked centrifugal interchange instability and (2) from precipitation to the atmosphere via the loss cone.

[25] 1. As discussed earlier, it seems likely that hotter plasma has a source in the outer magnetosphere and is transported radially inward via the centrifugal interchange instability (CII). During CII transport an outer magnetospheric flux tube (carrying hot tenuous plasma) changes places with a relatively cold and dense inner magnetospheric flux tube. As this hotter flux tube moves planetward its contained plasma gradient and curvature drifts as shown in Figure 1. These drifts are energy-dependent, with hot plasma drifting out of the interchanged flux tube more quickly than cold plasma. Thus as a hot outer magnetospheric flux tube moves inward, it becomes increasingly depleted of its hotter particles [*Southwood and Kivelson*, 1987; *Burch et al.*, 2005; *Hill et al.*, 2005], and therefore interchange can move colder plasma to lower L-values than hot plasma, leading naturally to the increasingly distant *Rc* with increasing energy observed.

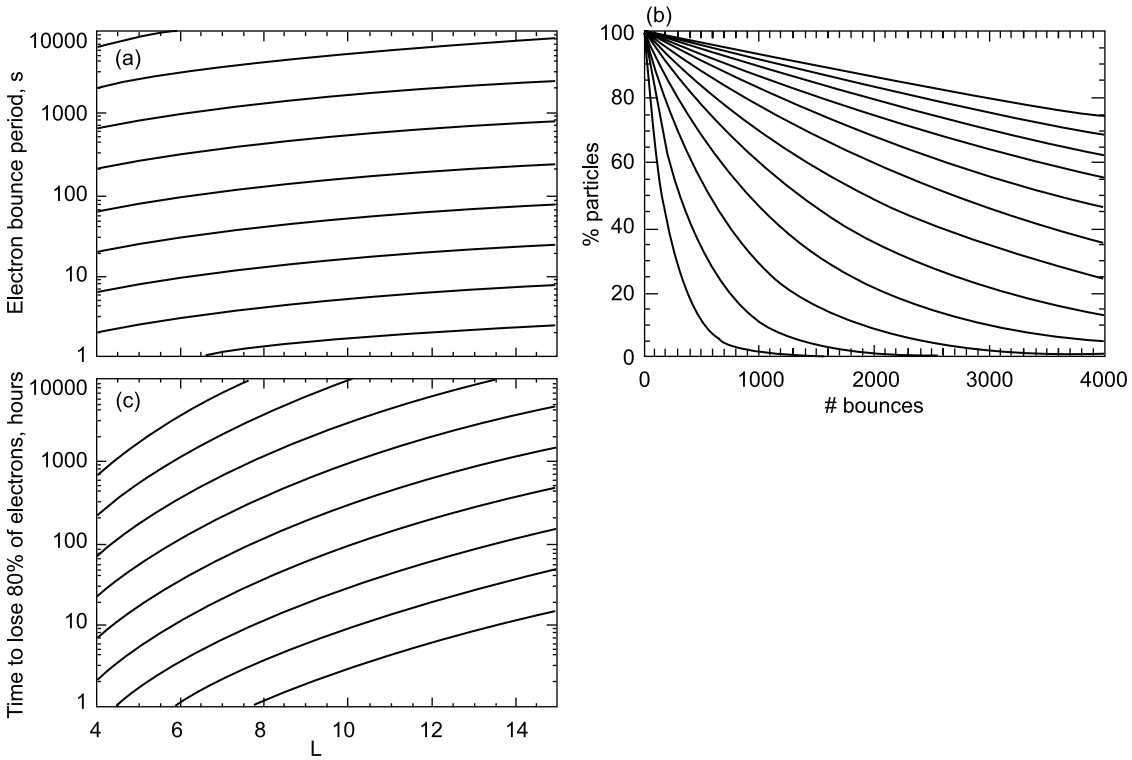

Figure 8. Clockwise from top left: (a) electron bounce period versus L for various electron energies; (b) percent of electrons remaining versus number of bounces at various L values; (c) time to lose 80% of electrons from the flux tube versus L for various electron energies, assuming the distributions are fully reisotropized each half bounce period. In Figures 8a and 8c the energy values range from (top) 0.1 eV to (bottom) 10 MeV, incremented by factors of 10 between curves. In Figure 8b the L values range from (bottom) 4 to (top) 15.

[26] 2. As electrons undergo bounce motion along magnetic field lines a portion of them will be lost through precipitation to the atmosphere via the loss cone twice per bounce period. The rate at which this process can evacuate the flux tube is dependent on energy, L value, and scattering efficiency, i.e., how quickly the loss cone volume can be repopulated. We can put an upper limit on how quickly electrons can be lost via the loss cone by assuming that electrons are efficiently scattered in their collisions, effectively randomizing them in pitch angle, i.e., strong pitch angle diffusion [*Lyons*, 1973]. In this case electrons can readily diffuse across the loss cone and the electron distributions reisotropize within a half bounce period. Figure 8a shows electron bounce period for various energies versus L, Figure 8b shows rate of loss in terms of number of bounces, and Figure 8c shows time to lose 80% of electrons versus L-shell. For example, the loss cone angle at $L = 6$ is approximately 3°. Given our assumption of strong scattering, it will take approximately 1300 bounce periods to lose 80% of particles from $L = 6$ through precipitation in the loss cone. This value corresponds to 30 hours for a 1 keV electron, about 300 hours for a 10 eV electron, and only 0.3 hours for a 10 MeV electron. Note these calculations represent upper limits only: our assumption that the electrons attain full isotropy in half a bounce period depends on how efficiently the electrons are scattered.

[27] Inside Rc we observe $f(v)$ to display a positive slope, the gradient of which decreases with increasing energy. Owing to the presence of penetrating radiation we cannot currently resolve ELS thermal electrons inside $L \sim 5$ and so we are not able to specifically discern thermal electron sources/losses inside this distance. If we assume that the loss region (be it at a discrete L-shell or a distributed loss) is constant and that the region displaying a flat $f(v)$ profile is effectively "communicating" an external source to Rc, then the sloped $f(v)$ profile observed is consistent with the classical interpretation of an external source and an internal loss, as displayed in Figure 3a.

5. Conclusions

[28] We confirm the observations of *Sittler et al.* [1983] and *Young et al.* [2005] that there often exist two electron populations in the inner magnetosphere of Saturn, typically in the equatorial range $5 < L < 12$. We also confirm, as recognized by Young et al., that the energy of the cold plasmasphere-like population of electrons approximately tracks the proton corotation energy. We used the observed L dependence of phase space density at constant values of the isotropic invariant Λ [*Wolf*, 1983; *Schultz*, 1998] to test for sources and sinks of these two electron populations separately. We show that Λ has similar functional form to that of the first isotropic invariant μ and so the following conclusions apply to transport in terms of conservation of μ or Λ.

[29] Our analysis suggests that there exists a distributed source of low-energy (<100 eV) electrons inside $L \sim 11$. Observations presented here and by *Young et al.* [2005] are consistent with the thermal electrons and ions being pickup products following the ionization of neutrals from Saturn's neutral cloud. This process almost instantaneously forms an ion at the ion corotation energy and a much colder electron (~<1eV). We suggest that, given sufficiently long residence times (slow plasma transport), the electrons can significantly equilibrate with the ions through Coulomb collisions. Because the energization of the electrons violates the electron adiabatic invariant, the heating process looks like an electron source in our phase space density analyses. Our estimate for the plasma transport timescale (~300 hours) is on the order of our estimate for time required for ions and electrons to approach temperature equilibration through Coulomb collisions (~150 hours). Given the rough estimates used, local electron heating through Coloumb collisions cannot be ruled out.

[30] Since the cold electron source is ultimately linked to Saturn's neutral cloud then we might expect to see a peak in the cold electrons at the orbit of Enceladus; we are unable to resolve such a peak at present.

[31] Investigating higher values of the isotropic invariant, Λ, we test for sources and losses of the hot electron component. We find that the average energy of the "hot" (100 eV to >10 keV) electron component increases with decreasing L-shell in a way that is consistent with conservative transport. This is consistent with inward transport of outer magnetospheric flux tubes driven by the centrifugal interchange instability, although the cold outflowing counterpart of this process is more difficult to identify. If the dominant source of inner magnetospheric neutrals (and therefore plasma) is the venting observed from Enceladus, then we might expect to observe interchange all the way to $L = 4$. However, we observe that hot electrons undergo heavy losses inside Dione's orbit at $L \sim 6$, presumably due to interaction with Saturn's neutral cloud or E-ring (although a few strong injection events are observed inward of this point). We observe that the distance *Rc* to which the hot electron component penetrates into the neutral cloud is energy-dependent, with the coolest fraction of the hot plasma (E ~ 100 eV) penetrating to the lowest L-shells. This result suggests that either cooler plasma is transported radially inward more efficiently than hot plasma and/or hot plasma is more readily lost inside *Rc* than cooler plasma. Our conjecture is that this arises naturally due to energy-dependent transport by interchange and/or loss through precipitation in the loss cone. If the transport is due to the centrifugal interchange instability, CII, then we suggest that this energy dependence arises as hot plasma gradient and curvature drifts out of the inwardly moving flux tubes more efficiently than does the cold plasma and so the CII can transport cold plasma inward more efficiently than hot. Consistent with our assumption of strong scattering (inherent in the use of the isotropic invariant) is the assumption that the plasma undergoes strong pitch angle diffusion, and so the electron distributions approximately isotropize in a bounce period. This situation presents an additional energy-dependent loss process as higher-energy electrons precipitate via the loss cone; for example, at $L = 6$ this corresponds to a loss of 80% of the electrons in ~1300 bounces.

[32] Inside *Rc* we see the almost complete absence of hot electrons (although a few fairly short-lived dispersion events are still evident and should be explored in more detail in future work). The $f(v)$ profile falls off sharply inward of *Rc* consistent with the classical picture of an external electron source and an internal loss probably due to scattering losses that increase both with the increasing loss cones associated with decreasing values of L and perhaps that increase as a result of increasing low-energy plasma densities that can stimulate wave activity.

[33] **Acknowledgments.** We thank the many individuals at JPL and NASA who have contributed to making the Cassini project an outstanding success. This work was supported by NASA JPL contract 1243218 to Southwest Research Institute for the Cassini CAPS investigation and by NASA JPL contract to the Johns Hopkins University Applied Physics Laboratory for the Cassini MIMI investigation.

[34] Wolfgang Baumjohann thanks the reviewers for their assistance in evaluating this paper.

References

André, N., M. K. Dougherty, C. T. Russell, J. S. Leisner, and K. K. Khurana (2005), Dynamics of the Saturnian inner magnetosphere: First inferences from the Cassini magnetometers about small-scale plasma transport in the magnetosphere, *Geophys. Res. Lett.*, *32*, L14S06, doi:10.1029/2005GL022643.

Armstrong, T. P., E.V. Bell II, M. T. Paonessa, and S. M. Krimigis (1983), Voyager observations of Saturnian ion and electron phase space densities, *J. Geophys. Res.*, *88*, 8893–8904.

Barbosa, D. D. (1990), Radial diffusion of low-energy plasma ions in Saturn's magnetosphere, *J. Geophys, Res.*, *95*, 17,167–17,177.

Belcher, J. W., R. L. McNutt, J. D Richardson, R.S. Selesnick, E.C. Sittler, and F. Bagenal (1991),The plasma environment of Uranus, in *Uranus*, edited by J. T. Bergstrahlet al., pp. 780–830, Univ. of Ariz. Press, Tucson, Ariz.

Book, D. L. (1981), *A Physicist's Desk Reference*, 2nd ed., edited by H. L. Anderson, 281 pp., Am. Inst. of Phys., New York.

Burch, J. L., J. Goldstein, T. W. Hill, D. T. Young, F. J. Crary, A. J. Coates, N. Andre, W. S. Kurth, and E. C. Sittler (2005), Properties of local plasma injections in Saturn's magnetosphere, *Geophys. Res. Lett.*, *32*, L14S02, doi:10.1029/2005GL022611.

Dougherty, M. K., et al. (2004), The Cassini magnetic field investigation, *Space Sci. Rev.*, *114*, 331–383.

Feldman, W. C., J. R. Ashridge, S. J. Bame, M. D. Montgomery, and S. P. Gary (1975), Solar wind electrons, *J. Geophys. Res.*, *80*, 4181.

Frank, L. A., and W. R. Paterson (2000), Observations of plasmas in the Io torus with the Galileo spacecraft, *J. Geophys. Res.*, *105*, 16,017–16,034.

Green, J. C., and M. G. Kivelson (2004), Relativistic electrons in the outer radiation belt: differentiating between acceleration mechanisms, *J. Geophys. Res.*, *109*, A03213, doi:10.1029/2003JA010153.

Gurnett, D. A., et al. (2005), Radio and Plasma Wave observations at Saturn from Cassini's approach and first orbit, *Science*, *307*, 1255–1259.

Hansen, C. J., L. Esposito, A. I. F. Stewart, J. Cowell, A. Hendrix, W. Pryor, D. Shemansky, and R. West (2006), Enceladus' water vapour plume, *Science*, *311*, 1422–1425.

Hill, T. W., A. M. Rymer, J. L. Burch, F. J. Crary, D. T. Young, M. F. Thomsen, D. Delapp, N. André, A. J. Coates, and G. R. Lewis (2005), Evidence for rotationally-driven plasma transport in Saturn's magnetosphere, *Geophys. Res. Lett.*, *32*, L14S10, doi:10.1029/2005GL022620.

Huang, T. S., and T. W. Hill (1991), Drift wave instability in the Io plasma torus, *J. Geophy. Res.*, *96*, 14,075–14,083.

Johnson, R. E., M. Liu, and E. C. Sittler (2005), Plasma-induced clearing and redistribution of material embedded in planetary magnetospheres, *Geophys. Res. Lett.*, *32*, L24201, doi:10.1029/2005GL024275.

Johnson, R. E., H. T. Smith, O. J. Tucker, M. Liu, M. H. Burger, E. C. Sittler, and R. L. Tokar (2006), The Enceladus and OH tori at Saturn, *Astrophys. J.*, *644*, 137–139.

Jurac, S., and J. D. Richardson (2005), A self-consistent model of plasma and neutrals at Saturn: Neutral cloud morphology, *J. Geophys. Res.*, *110*, A09220, doi:10.1029/2004JA010635.

Jurac, S., M. A. McGrath, R. E. Johnson, J. D. Richardson, V. M. Vasyliunas, and A. Eviatar (2002), Saturn: Search for a missing water source, *Geophys. Res. Lett.*, *29*(24), 2172, doi:10.1029/2002GL015855.

Krimigis, S. M., et al. (2004), Magnetosphere Imaging Instrument (MIMI) on the Cassini Mission to Saturn/Titan, *Space Sci. Rev.*, *114*, 233–329.

Leisner, J. S., C. T. Russell, K. K. Khurana, M. K. Dougherty, and N. André (2005), Warm flux tubes in the E-ring plasma torus: Initial Cassini magnetometer observations, *Geophys. Res. Lett.*, *32*, L14S08, doi:10.1029/2005GL022652.

Linder, D. R., et al. (1998), The Cassini CAPS electron spectrometer, in *Measurement Techniques in Space Plasmas: Particles*, *Geophys Monogr. Ser.*, vol. 102, edited by R. F. Pfaff, J. E. Borovsky, and D. T. Young, p. 257, AGU, Washington, D. C.

Lundin, R. (1988), On the magnetospheric boundary layer and solar wind energy transfer into the magnetosphere, *Space Sci. Rev.*, *48*, 263–320.

Lyons, L. R. (1973), Comments on pitch angle diffusion in the radiation belts, *J. Geophys. Rev.*, *78*, 6793.

Mauk, B. H., et al. (2005), Energetic particle injections in Saturn's magnetosphere, *Geophys. Res. Lett.*, *32*, L14S05, doi:10.1029/2005GL022485.

Maurice, S., E. C. Sittler, J. F. Cooper, B. H. Mauk, M. Blanc, and R. S. Selesnick (1996), Comprehensive analysis of electron observations at Saturn: Voyager 1 and 2, *J. Geophys. Res.*, *101*, 15,211–15,232.

McDonald, F. B., A. W. Schardt, and J. H. Trainor (1980), If you've seen one magnetosphere, you haven't seen them all: Energetic particle observations in the Saturn magnetosphere, *J. Geophys. Res.*, *85*, 5813–5830.

Mitchell, R. (2000), The Cassini/Huygens mission to Saturn, tech. rep., Jet Propulsion Lab., Calif. Inst. of Tech., Pasadena, Calif.

Pontius, D. H., Jr., and T. W. Hill (2006), Enceladus: A significant plasma source for Saturn's magnetosphere, *J. Geophys. Res.*, *111*, A09214, doi:10.1029/2006JA011674.

Porco, C. C., et al. (2006), Cassini observes the active south pole of Enceladus, *Science*, *311*, 1393–1401.

Richardson, J. D. (1986), Thermal ions at Saturn: Plasma parameters and implications, *J. Geophys. Res.*, *91*, 1381–1389.

Richardson, J. D. (1992), A new model for plasma transport and chemistry at Saturn, *J. Geophys. Res.*, *97*, 13,075–13,713.

Richardson, J. D., and G. L. Siscoe (1981), Factors governing the ratio of inward to outward diffusing flux of satellite ions, *J. Geophys. Res.*, *86*, 8485–8490.

Richardson, J. D., and E. C. Sittler (1990), A plasma density model for Saturn based on Voyager observations, *J. Geophys. Res.*, *95*, 12,019–12,031.

Richardson, J. D., A. Eviatar, M. A. McGrath, and V. M. Vasyliunas (1998), OH in Saturn's magnetosphere: Observations and implications, *J. Geophys. Res.*, *103*, 20,245–20,256.

Rymer, A. M. (2004), Analysis of Cassini plasma and magnetic field measurements from 1–7 AU, Ph.D. thesis, Univ. College London, London, UK.

Schulz, M. (1998), Particle drift and loss rates under strong pitch angle diffusion in Dungey's model magnetosphere, *J. Geophys. Res.*, *103*, 61–68.

Scudder, J. D., E. C. Sittler, and H. S. Bridge (1981), A survey of the plasma electron environment of Jupiter: A view from Voyager, *J. Geophys. Res.*, *86*, 8157–8179.

Sittler, E. C., Jr., and D. F. Strobel (1987), Io plasma torus electrons: Voyager 1, *J. Geophys. Res.*, *92*, 5741–5762.

Sittler, E. C., Jr., K. W. Ogilvie, and J. D. Scudder (1983), Survey of low-energy plasma electrons in Saturn's magnetosphere: Voyager 1 and 2, *J. Geophys. Res.*, *88*, 8847–8870.

Sittler, E. C., Jr., et al. (2005), Preliminary results on Saturn's inner plasmasphere as observed by Cassini: Comparison with Voyager, *Geophys. Res. Lett.*, *32*, L14S07, doi:10.1029/2005GL022653.

Sittler, E. C., Jr., et al. (2006), Cassini observations of Saturn's inner plasmasphere: Saturn orbit insertion results, *Planet. Space Sci.*, *54*, 1197–1210.

Southwood, D. J., and M. G. Kivelson (1987), Magnetospheric interchange instability, *J. Geophys., Res.*, *92*, 109–116.

Spahn, F., et al. (2006), Cassini dust measurements at Enceladus and implications for the origin of the E ring, *Science*, *311*, 1416–1418.

Spitzer, L. (1962), *Physics of Fully Ionized Gases*, 2nd ed., Wiley-Interscience, Hoboken, N. J.

Tokar, R. L., et al. (2006), The interaction of the atmosphere of Enceladus with Saturn's plasma, *Science*, *311*, 1409, doi:10.1126/science.1121061.

Van Allen, J. A., B. A. Randall, and M. F. Thomsen (1980), Sources and sinks of energetic electrons and protons in Saturn's magnetosphere, *J. Geophys. Res.*, *85*, 5679–5694.

Waite, J. H., Jr., et al. (2006), Ion and Neutral Mass Spectrometer: Enceladus plume composition and structure, *Science*, *311*, 1419–1422.

Wolf, R. A. (1983), The quasi-static (slow-flow) region of the magnetosphere, in *Solar-Terrestrial Physics: Principles and Theoretical Foundations*, pp. 303–368, Springer, New York.

Young, D. T., et al. (2004), Cassini Plasma Spectrometer investigation, *Space Sci. Rev.*, *114*, 1–112.

Young, D. T., et al. (2005), Composition and dynamics of plasma in Saturn's magnetosphere, *Science*, *307*, 1262–1266.

N. André, Research and Scientific Support Department, European Space Research and Technology Centre, Keperlaan 1, Postbus 299, 2200 AG Noordwijk, Netherlands.

S. J. Bolton and D. T. Young, Southwest Research Institute, 6220 Culebra Road, San Antonio, TX 78238, USA.

A. J. Coates, Mullard Space Science Laboratory, University College London, Dorking Surrey, RH5 6NT, UK.

M. K. Dougherty, Department of Space and Atmospheric Physics, Imperial College London, Queen's Gate, London, SW7 2RH, UK.

T. W. Hill, Department of Physics and Astronomy, Rice University, Houston, TX 77005, USA.

R. E. Johnson and H. T. Smith, University of Virginia, Charlottesville, VA 22904, USA.

B. H. Mauk, D. G. Mitchell, C. Paranicas, and A. M. Rymer, Johns Hopkins University Applied Physics Laboratory, Laurel, MD 20723, USA. (abigail.rymer@jhuapl.edu)

E. C. Sittler Jr., NASA Goddard Space Flight Center, Greenbelt, MD 20770, USA.

M. F. Thomsen, Space and Atmospheric Science Group, Los Alamos National Laboratory, Los Alamos, NM 87545, USA.